A petrological experiment on Emeishan basalt: Implications for the formation of syenite from the Baima igneous complex

Wen-Yu Hsia[1], J. Gregory Shellnutt[1, *], Teh-Ching Liu[1], and Yoshiyuki Iizuka[2]

[1] *National Taiwan Normal University, Department of Earth Sciences, Taipei City, Taiwan*
[2] *Institute of Earth Sciences, Academia Sinica, Taipei City, Taiwan*

ABSTRACT

The Baima igneous complex (BIC) consists of a cumulate layered gabbroic unit, an Fe-Ti oxide ore zone, and an isotropic quartz syenite. The formation of the BIC is attributed to a variety of petrological processes including: silicate immiscibility, fractional crystallization, and fluxing of fO_2 by either internal or external factors. This study attempts to determine if a parental magma similar to high-Ti Emeishan basalt can produce the syenitic rocks of the BIC. The experimental results at atmospheric pressure show that the liquidus temperature and solidus temperature of the basaltic melt are estimated to be 1303 and 1120°C. The crystallization sequence is: titanomagnetite, clinopyroxene ($Wo_{43-47}En_{32-45}Fs_{11-23}$), and plagioclase ($An_{65-31}$). The residual liquid composition, represented by quenched glass, evolves from lower SiO_2 (~45 wt%) values to higher values (~60 wt%) with corresponding decreases in Ti, Fe, Mg, Ca and increases of Na and K. The results show that a starting composition of high-Ti basalt from the Emeishan large igneous province can produce evolved silicic liquids that resemble the compositions of microgranular enclaves from the Baima syenitic unit.

1. INTRODUCTION

The current understanding of magma chamber processes is derived from observations of layered mafic-ultramafic intrusions preserved in the geological record and physical observations deduced from geophysical surveys at volcanic centers (Wager and Brown 1968; Iyer 1984; Cawthorn 1996; Murru et al. 1999; Charlier et al. 2015; Mondal and Griffin 2017). Many layered intrusions are of significant economic importance as they host world class deposits of precious (PGE, Au, Ag) and base (Fe, Ni, Zn) metals. Therefore, constraining the processes that enrich layered intrusions in precious and/or base metals is of primary importance for mineral exploration (Lee 1996). Specifically, the formation of magmatic Fe-Ti-V oxide deposits is not well understood although many occur in the upper, more differentiated units of layered intrusions whereas the lower units commonly have Cr- and PGE-rich horizons (e.g., Bushveld Complex, Stillwater Complex).

Fractional crystallization, magma mingling, silicate liquid immiscibility, separate magma systems, and oxygen fugacity (fO_2) fluxing are suggested as possible processes which induce metal enrichment but there remains a large degree of uncertainty. It appears that there is no general model that can be applied to all deposits associated with layered intrusions but rather there are specific conditions unique to each deposit that may be important to their formation (Philpotts 1967; Cawthorn 1996; Lee 1996; Duchesne 1999; Van Tongeren and Mathez 2012; Charlier et al. 2015). Furthermore, many layered intrusions are associated with silicic plutons that are similar to A-type (ferran) granitoids (Bonin 2007). The spatial and temporal association of silicic intrusions with layered ultramafic-mafic intrusions suggests they may be petrogenetically related and that the formation of Fe-Ti oxide deposits is a consequence of their cogenesis

* *Corresponding author*
 E-mail: jgshelln@ntnu.edu.tw

(Shellnutt et al. 2009, 2011; Shellnutt and Jahn 2010; Zhong et al. 2011).

The middle-Late Permian (~260 Ma) Emeishan large igneous province (ELIP) of southwestern China is located along the western margin of the Late Archean to Early Proterozoic Yangtze Block. The ELIP covers an area of ~0.5 × 10^6 km^2 and consists principally of continental flood basalts but there are a number of mafic-ultramafic intrusions, some of which host giant Fe-Ti-V oxide deposits and/or Ni-Cu-(PGE) sulphide deposits (Ali et al. 2005; Zhong et al. 2005; Song et al. 2006, 2013; Wang et al. 2007; Zhou et al. 2008; Pang et al. 2010; Shellnutt 2014; Pang and Shellnutt 2017). The oxide-bearing layered ultramafic-mafic complexes are concentrated within the west-central part of the ELIP known as the Panxi region (Panzhihua-Xi Chang). The layered complexes can be divided into two main groups: (1) ultramafic-mafic and (2) mafic. The ultramafic-mafic intrusions typically consist of a lower olivine- and pyroxene-rich peridotite unit which grades into a plagioclase-bearing upper gabbroic unit whereas the mafic layered intrusions consist of gabbro with varying proportions of olivine, clinopyroxene, plagioclase, and titanomagnetite across all layers (Zhong et al. 2002; Zhou et al. 2005; Wang et al. 2007; Pang et al. 2010; Shellnutt et al. 2011, 2015; Pêcher et al. 2013; Song et al. 2013; Bai et al. 2014; She et al. 2014; Pang and Shellnutt 2017). The primary difference between the two groups is the type and style of mineralization. The mafic-ultramafic intrusions have PGE-rich horizons in their lower parts and Fe-Ti-oxide deposits in their middle to upper layers (e.g., Hongge). In contrast the mafic intrusions strictly have Fe-Ti oxide deposits (e.g., Panzhihua, Taihe, Baima) in their lower layers (Zhou et al. 2008; Pang et al. 2010). Another difference between the two types of layered intrusions is that the mafic intrusions are spatially and temporally associated with peralkaline A-type granitoids whereas the ultramafic-mafic intrusions are not. The petrogenetic relationship between the mafic intrusions and the peralkaline granitic intrusions is a contentious issue and is focused on whether or not the spatially associated mafic and silicic rocks are members of the same complex (Shellnutt et al. 2011; Zhong et al. 2011; Zhang et al. 2012). Additionally the formation of the Fe-Ti oxide deposits within the mafic intrusions are considered to be derived by a number of processes such as: silicate liquid immiscibility, fractional crystallization or fO$_2$ fluxing by carbonate country rock assimilation from either a mafic or ultramafic parental magma (Zhou et al. 2005, 2013; Ganino et al. 2008; Pang et al. 2008a, b, 2009; Zhang et al. 2009, 2012; Shellnutt et al. 2011, 2015; Zhong et al. 2011; Song et al. 2013; Liu et al. 2014a, b, 2016; She et al. 2014; Bai et al. 2016; Chen et al. 2017; Tang et al. 2017; Xing et al. 2017).

In this paper we present the results of low pressure (atmospheric), anhydrous equilibrium crystallization experiments on a 'high-Ti' Emeishan basalt composition in order to determine if the syenitic unit of the Baima igneous complex can be derived from a mafic parental magma. Moreover, the results of this study have implications for the formation of orthomagmatic Fe-Ti oxide deposits of the Panxi region.

2. PETROLOGY OF THE BAIMA IGNEOUS COMPLEX

The Baima igneous complex (BIC) is located in the central part of the Panxi region, ~100 km northeast of Panzhihua city, and consists of a gabbroic unit, a syenitic unit and massive oxide ore deposit (Fig. 1). The layered gabbroic unit lies to the east of the syenitic unit and dips ~23 to 27° to the west and is estimated to contain 1150 Mt of Fe, 44.8 Mt of Ti, and 2.85 Mt of V (Zhong et al. 2005). The two units appear to cover an area of similar size, but their respective volumes are unknown. Zircon U-Pb SHRIMP ages of 258 ± 4 Ma and 259 ± 5 Ma of the syenitic unit are within error of the 261 ± 2 Ma of the gabbroic unit (Shellnutt et al. 2009). It is thought that the layered intrusive rocks and the syenites are comagmatic and cogenetic (Yang et al. 1997; Shellnutt et al. 2009; Zhong et al. 2011; Liu et al. 2014a).

The gabbroic unit can be divided into four lithologic zones from the bottom to the top: (1) a lower cumulate zone; (2) an oxide ore zone; (3) an olivine gabbro zone; and (4) an upper gabbro zone (Chen 1990) (Fig. 2). The rocks from the four zones consist of coarse grained cumulus olivine, plagioclase, clinopyroxene, and interstitial Fe-Ti oxide minerals with minor amounts of sulphide minerals, spinel (pleonaste), and apatite (Chen 1990; Shellnutt and Pang 2012; Liu et al. 2014a; Chen et al. 2014). The upper zone tends to have less olivine and more apatite than the lower cumulate zone and the olivine gabbro zone. The ore deposits are hosted within the lower portions of the layered cumulate gabbro (Chen 1990; Shellnutt et al. 2009).

The syenite is coarse grained, granular and consists of perthitic alkali feldspar, sodic amphibole, quartz, aegirine and accessory amounts (≤ 5 vol %) of apatite, titanite, zircon, plagioclase, fluorite, biotite, ilmenite, magnetite, and pyrite (Shellnutt and Iizuka 2011). The syenitic unit is structurally above the gabbroic unit and contains ellipsoidal microgranular enclaves varying in size from a few centimeters to 10s of centimeters in length (Shellnutt et al. 2010). There are a few small lenticular zones of finer grained textures which are more siliceous in composition. All units of the BIC were intruded by alkaline mafic dykes (257.6 ± 0.5 Ma to 259.5 ± 0.8 Ma) whereas the petrogenetically unrelated Woshui syenite (259.6 ± 0.5 Ma) and Huangcao syenite (258.9 ± 0.7 Ma) intruded the margins of the BIC (Shellnutt and Zhou 2007, 2008; Shellnutt et al. 2008, 2012; Shellnutt and Iizuka 2011).
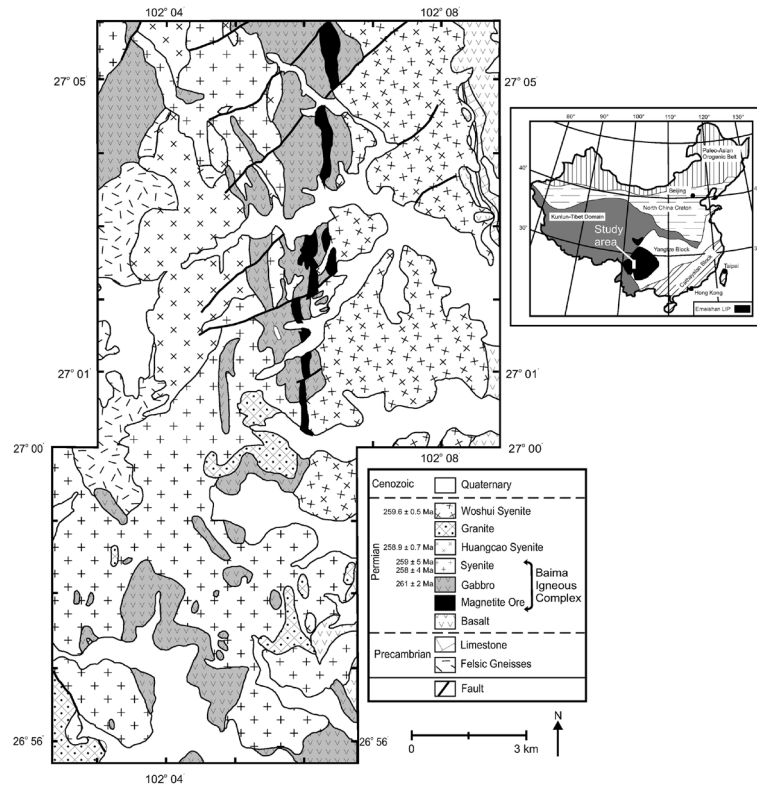
Fig. 1. Simplified geological map showing the distributions of the major units of the BIC (modified from Wang et al. 1994 and Xiong et al. 1996). Zircon U-Pb age dates from Shellnutt et al. (2009, 2012).
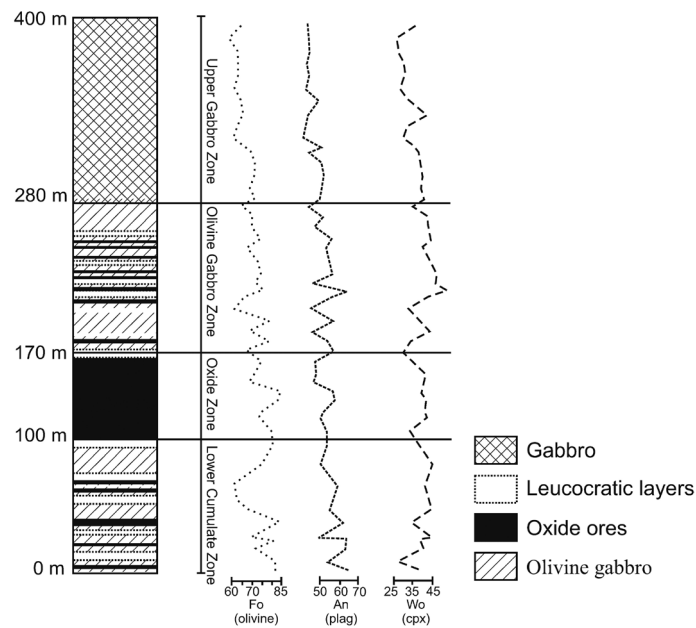

Fig. 2. The stratigraphic column of the layered gabbro of the BIC showing the different facies based on Chen (1990). Mineral chemical variations after Chen (1990) are shown for reference. Fo = forsterite value, An = anorthite value, Wo = wollastonite value.

3. STARTING COMPOSITION AND EXPERIMENTAL SET-UP

3.1 Starting Composition

Previous studies have suggested that the parental magma composition of the BIC was similar to the high-Ti Emeishan basalt (Shellnutt et al. 2009), specifically sample EM-81 reported by Xu et al. (2001). In this study, we selected a known composition of Emeishan high-Ti basalt from the Baima area as the parental magma of the BIC syenite (Table 1). Sample GS04-026 was collected from a mafic dyke with chilled margins that intruded the syenitic portion of the BIC and is reported by Shellnutt et al. (2008). The bulk composition of GS04-026 is similar to EM-81 but there are some minor differences with respect to the Al_2O_3, Fe_2O_3, and Na_2O contents (Table 1). Given the low MgO (< 8 wt%) and CaO (< 12.0 wt%) contents of GS04-026, it is probably not representative of a primary melt but likely that it experienced crystal fractionation (e.g., olivine, ± clinopyroxene ± plagioclase) prior to emplacement.

3.2 Experimental Conditions

The rock powder was encased in closed platinum envelopes and was suspended in a 1-atm vertical-quenching furnace. The samples were melted at the desired temperature. All temperatures were measured using an R-type thermocouple (Pt-Pt$_{87}$Rh$_{13}$ thermocouple) and were corrected to the International Practical Temperature Scale of 1968 based on the calibration with the melting point of synthetic diopside ($CaMgSi_2O_6$). The precision of the thermocouple is ±1°C. The experimental duration in this study ranged from 6 to 47.5 hours at temperatures from 1305 to 1125°C. At the end of each run, the products were quenched in water. The complete results of the low pressure experiments can be found in Table S1 of the online supplementary files. The total FeO of the starting material is 14.83 wt%. The total FeO of the glass melted at 1310°C and atmospheric pressure for six hours is 14.67 wt%. The difference between them is ~1% and therefore, the iron loss to the Pt envelope at atmospheric pressure was negligible.

4. ANALYTICAL METHODS

4.1 Electron Probe Micro Analyzer

After quenching, the experimental charges were mounted in epoxy and polished to make a section for mineral analysis. The mineralogical investigation was carried out by an electron probe micro analyzer (JEOL EPMA JXA-8900R) equipped with four wave-length dispersive spectrometers (WDS) at the Institute of Earth Sciences, Academia Sinica in Taipei. Secondary- and back-scattered electron images were taken of each sample and used to select specific minerals for analysis. A 2 μm defocused beam

Table 1. Composition of starting material, EM-81 and average high-Ti Emeishan basalt.

Element	GS04-026	EM-81	High-Ti$_{avg}$
SiO$_2$ (wt%)	45.01	44.51	47.52
TiO$_2$	3.97	3.47	3.44
Al$_2$O$_3$	12.42	13.75	13.33
Fe$_2$O$_3$t	16.48	16.37	14.20
MnO	0.24	0.22	0.20
MgO	5.89	6.93	5.61
CaO	10.16	10.15	8.96
Na$_2$O	3.23	2.40	2.67
K$_2$O	1.34	1.08	1.17
P$_2$O$_5$	0.30	0.35	0.43
Total	99.04	99.23	97.06
Sc (ppm)	33		
V	893	438	
Cr	26	98	
Co	57	52	
Ni	61	86	
Cu	333	209	
Zn	158	121	
Ga	23	26	
Rb	62	35	
Sr	401	780	
Y	26	35	
Zr	165	227	
Nb	21	31	
Cs	0.7		
Ba	310	590	
La	24.5	29.6	
Ce	54.2	63.8	
Pr	7.2		
Nd	30.5	35.9	
Sm	6.8	8.5	
Eu	2.2	2.8	
Gd	6.0		
Tb	1.0	1.1	
Dy	5.5		
Ho	1.0		
Er	2.8		
Tm	0.4		
Yb	2.3	2.3	
Lu	0.3	0.3	
Hf	4.6	5.8	
Ta	1.5	1.7	
Th	3.2	0.7	
U	0.8	0.3	

or a focused beam were operated for quantitative analysis at an acceleration voltage of 15 kV and beam current of 12 nA. The measured X-ray intensities were corrected by ZAF method using the standard calibration of synthetic chemical-known standard minerals with various diffracting crystals that included: diopside or wollastonite for Si with TAP crystal, rutile for Ti with PET crystal, corundum for Al (TAP), chromium oxide for Cr (PET), fayalite or hematite for Fe with LiF crystal, tephroite for Mn (PET), periclase for Mg (TAP), wollastonite for Ca (PET), albite for Na (TAP), and adularia for K (PET). Peak counting for each element and both upper and lower baseline X-rays are counted for 10 and 5 s, respectively. Standard reference materials yielded relative standard deviations of < 1% for Si, Na and K, and < 0.5% for other elements.

4.2 Laser Ablation (LA) Inductively Coupled Mass Spectrometry (ICP-MS)

The trace elements were measured by inductively coupled plasma-mass spectrometry (ICP-MS) using an Agilent 7500s quadrupole spectrometer at the Department of Geosciences, National Taiwan University. The laser ablation was performed with a helium carrier gas and spot size of ablation was 30 μm, with laser repetition rate and laser energy density being 4 Hz and of 10 J cm^{-2}, respectively. The USGS glass (NIST 610) was used as the external standard and BCR-2 was also used as secondary standard for verification of analytical results. Calcium (determined by EPMA) was used as the internal normalization standard for

the glass. All concentrations were calculated using GLITTER 4.0 (GEMOC) software. The measured results of NIST 610 and BCR-2 are in supplementary Table S2 together with literature reference values. The precision of ~30 trace elements measured is generally better than 10%.

5. RESULTS

The temperature range for the low pressure experiments was 1310 to 1125°C with a liquidus temperature of ~1303°C whereas the solidus temperature is estimated to be ~1120°C. The complete crystallization sequences for each experiment are shown in Table 2 but the overall crystallization sequence is iron-titanium (Ti-rich magnetite) oxide at 1303°C, clinopyroxene at 1184°C, and plagioclase at 1162°C (Fig. 3).

The average compositions of the iron-titanium oxides for each experiment are listed in Table 3. The bulk FeOt content of the oxides, at high temperature, ranges from ~75 to ~65 wt% for all compositions with calculated FeO content from 31.7 to 36.2 wt%, Fe_2O_3 from 36.1 to 46.6 wt%, and TiO_2 from 9.8 to 15.8 wt%. The lowest temperature run produced both Ti-rich magnetite and ilmenite but the former was more abundant than the latter (Fig. 3).

The average clinopyroxene compositions are listed in Table 4. The wollastonite (Wo) component of the pyroxenes ranges from 49.4 to 44.3 mol. %; the enstatite (En) component ranges from 45.2 to 32.9 mol. %; and the ferrosilite (Fs) component ranges from 20.7 to 8.6 mol. %. The clinopyroxene classifies as diopside-augite (Fig. 4). The TiO_2

Table 2. Experimental conditions and crystallization history.

Run	Pressure	Temp (°C)	Time (h:m)	Phases
BM-023	1 atm	1310	6:00	gl
BM-028	1 atm	1305	6:10	gl
BM-005	1 atm	1300	6:10	gl + mt
BM-018	1 atm	1294	22:00	gl + mt
BM-015	1 atm	1286	21:00	gl + mt
BM-014	1 atm	1275	26:50	gl + mt
BM-004	1 atm	1250	19:30	gl + mt
BM-003	1 atm	1198	47:30	gl + mt
BM-024	1 atm	1187	17:40	gl + mt
BM-026	1 atm	1180	19:00	gl + mt + px
BM-008	1 atm	1173	20:34	gl + mt + px
BM-022	1 atm	1165	38:20	gl + mt + px
BM-027	1 atm	1159	21:00	gl + mt + px + pl
BM-001	1 atm	1151	17:20	gl + mt + px + pl
BM-007	1 atm	1125	19:50	gl + mt + il + px + pl

Note: h:m = hours:minutes; gl = glass, mt = magnetite, px = clinopyroxene, pl = plagioclase, il = ilmenite.
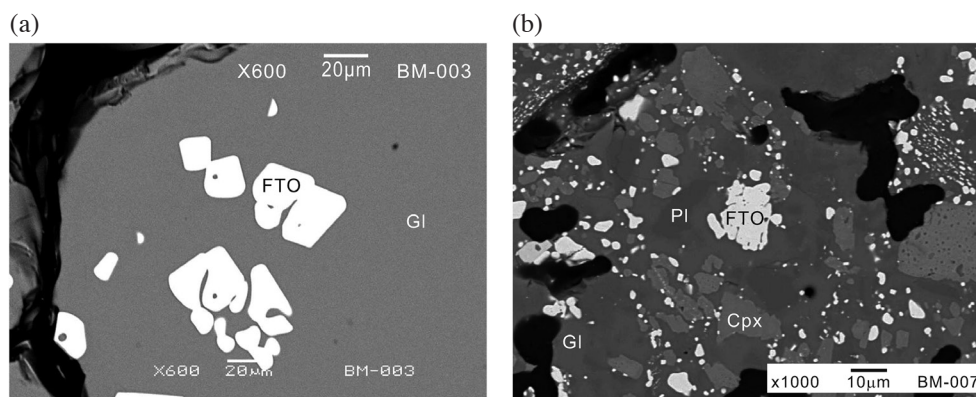
Fig. 3. Scanning electron microscopy images. (a) Crystallization of magnetite structured spinel at 1198°C. (b) Crystallization of diopside-augite and plagioclase at 1125°C.

Table 3. Average composition of the magnetite and ilmenite.

Sample	BM-005	BM-026	s.d.	BM-027	s.d.	BM-007	s.d.	BM-007	s.d.	Baima*
Temp. (°C)	1300	1180	(8)	1159	(9)	1125	(5)	1125	(3)	PO
SiO_2 (wt%)	0.01	0.03	0.02	0.09	0.09	0.00				
TiO_2	9.79	12.72	0.25	13.76	0.44	14.51	1.87	44.62	1.76	13.13
Al_2O_3	2.12	1.90	0.05	1.71	0.09	1.80	0.43	1.09	0.67	4.45
Cr_2O_3	0.06									
FeOT	75.91	71.54	0.60	70.06	0.58	68.55	1.68	40.27	2.13	
NiO	0.08	0.03	0.03	0.03	0.02	0.05	0.06	0.03	0.01	
MnO	0.11	0.20	0.04	0.25	0.06	0.35	0.07	0.18	0.10	0.49
MgO	3.32	5.32	0.11	5.90	0.25	6.04	0.28	5.97	1.12	1.89
Total	91.39	91.73		91.82		91.30		92.16		
Fe_2O_3	46.57	42.20	0.59	40.52	0.64	38.80	2.64	12.35	1.88	39.91
FeO	34.00	33.56	0.27	33.60	0.59	33.64	1.90	29.16	1.03	41.18
Total	96.06	95.96		95.88		95.19		93.40		
Si	0.001	0.001	0.00	0.004	0.003	0.000				
Al^{vi}	0.096	0.084	0.00	0.075	0.004	0.080	0.021	0.033	0.020	
Fe^{3+}	1.339	1.194	0.01	1.142	0.020	1.100	0.089	0.239	0.038	
Ti	0.281	0.360	0.01	0.388	0.012	0.410	0.045	0.864	0.028	
Cr	0.002									
Fe^{2+}	1.087	1.055	0.01	1.052	0.017	1.058	0.039	0.628	0.018	
Ni	0.003	0.001	0.00	0.001	0.001	0.002	0.002	0.003	0.004	
Mn	0.003	0.006	0.00	0.008	0.002	0.011	0.003	0.004	0.002	
Mg	0.189	0.298	0.01	0.330	0.014	0.339	0.011	0.229	0.042	

Note: TFeO = total Fe^{2+}. Averaged number of analyses in parentheses. Baima* is the calculated primary oxide (PO) composition from Shellnutt and Pang (2012).

Table 4. Average composition of the clinopyroxene.

Sample	BM-026	s.d.	BM-027	s.d.	BM0-007	s.d.
Temp. (°C)	1180	(3)	1159	(7)	1125	(8)
SiO_2 (wt%)	46.29	0.51	48.19	1.24	51.72	0.78
TiO_2	1.33	0.08	1.37	0.20	0.28	0.11
Al_2O_3	5.17	0.51	4.35	0.63	1.12	0.81
FeO	9.59	0.24	8.34	1.14	11.33	0.88
MnO	0.15	0.01	0.24	0.06	0.32	0.04
MgO	13.59	0.30	14.58	1.25	11.60	0.38
CaO	22.20	0.26	22.12	0.16	21.44	0.77
Na_2O	0.67	0.08	0.65	0.07	0.78	0.26
K_2O	0.01	0.01	0.01	0.01	0.08	0.14
Total	99.00		99.85		98.66	
Cations on the Basis of 6O						
Si	1.774	0.018	1.830	0.041	1.981	0.015
Al^{iv}	0.226	0.018	0.165	0.048	0.019	0.015
Al^{vi}	0.007	0.006	0.006	0.006	0.031	0.033
Fe^{3+}	0.282	0.013	0.202	0.044	0.049	0.038
Ti	0.038	0.003	0.039	0.007	0.008	0.003
Fe^{2+}	0.018	0.016	0.042	0.044	0.312	0.042
Mn	0.005	0.001	0.008	0.002	0.011	0.002
Mg	0.777	0.013	0.825	0.057	0.662	0.020
Ca	0.912	0.014	0.901	0.033	0.880	0.040
Na	0.050	0.006	0.048	0.006	0.058	0.018
K	0.000	0.001	0.000	0.000	0.004	0.007
Wo	46	0.01	46	0.02	46	0.01
En	39	0.01	42	0.03	35	0.02
Fs	15	0.00	12	0.03	19	0.01

Note: Mineral symbols: En = Enstatite component; Fs = ferrosilite component; Wo = wollastonite component. s.d. = standard deviation. Number in parenthesis is the total number of analysis.
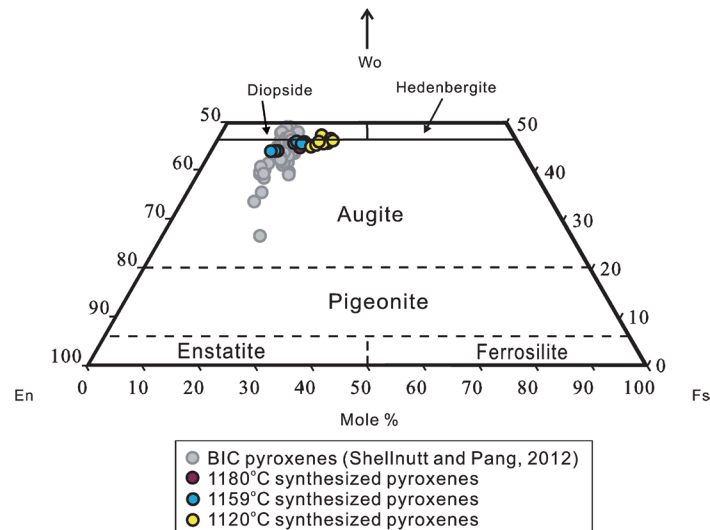

Fig. 4. Chemical classification of the experimental clinopyroxene in comparison to the clinopyroxene from the Baima layered gabbro.

content ranges from 0.2 to 1.7 wt% and the Al_2O_3 content ranges from 0.5 to 5.7 wt%.

The average composition of the plagioclase for each experiment ranges from labradorite (An_{65}) to andesine (An_{31}). The Al_2O_3 content is between 27.7 and 24.5 wt% whereas the K_2O content ranges from 0.25 to 0.63 wt% (Fig. 5; Table 5). The total iron, expressed as FeOt, ranges from 2.6 wt% in the high temperature experiments to 0.4 wt% in the lowest temperature experiments.

The averaged compositions of the residual glass for each experiment are listed in Table 6. The variation of the major element chemistry of the glass compositions versus temperature are plotted in Fig. 6. As the temperature decreased, the liquid line of descent shows an increase in SiO_2, Al_2O_3, Na_2O, and K_2O and decrease in MgO, TiO_2, and total FeO. The CaO of the glass increased between 1305 and 1180°C and then decreased (lowest temperature). The crystallization trend shows that the residual liquid, as represented by the glass, became considerably depleted in TiO_2 and total FeO as the temperature dropped below 1305°C. The depletion was triggered by the crystallization of the Ti-rich magnetite. When the temperature reached 1180°C, the CaO and MgO contents of the residual liquids became depleted as a result of the crystallization of clinopyroxene (Fig. 6).

The averaged trace elemental compositions of the glass from each run are listed in Table 7. The concentrations of compatible elements of the residual glass are highly variable; for example: Sc (15.1 - 30.6 ppm), Ni (16.1 - 54.8 ppm), and Cr (3.8 - 26.1 ppm). The trace element evolution relative to silica of the glass is illustrated in Fig. 7. As

the SiO_2 content of the residual glasses increased (i.e., decrease in temperature) the amount of Ba, Rb, Sr, Nd, and Zr increased (Fig. 7). In comparison, the Ni and Cr decreased significantly between 1305 and 1159°C.

6. DISCUSSION

6.1 An Analogue for the Formation of the Baima Syenitic Unit?

The Baima syenitic unit is considered to be representative a residual liquid derived by factional crystallization of a basaltic parental magma equal to high-Ti Emeishan basalt whereas the Baima layered gabbroic intrusion is considered to be the accumulated solid resulting from the same parental magma or batches of magma (Yang et al. 1997; Shellnutt et al. 2009, 2011; Shellnutt and Pang 2012; Zhang et al. 2012). Geological, mineralogical, and petrological evidence indicates the intrusion formed at low pressure (~0.1 GPa) and the relative oxidation state of the magmas was probably equal to or above the fayalite-magnetite-quartz (ΔFMQ 0 to +2) buffer (Shellnutt et al. 2009; Shellnutt and Iizuka 2012; Zhang et al. 2012). It is likely that the parental magma contained volatiles (CO_2, F, Cl, and H_2O) due to the presence of titanite, bastnäsite, fluorite, and amphibole in the Baima syenite (Shellnutt et al. 2009; Shellnutt and Iizuka 2011, 2012).

The resultant Ti-rich magnetite, clinopyroxene, and plagioclase crystallization in the model shows that the residual glass compositions reach moderately high SiO_2 concentration ($\geq$ 56 wt%). However, the most evolved silicic
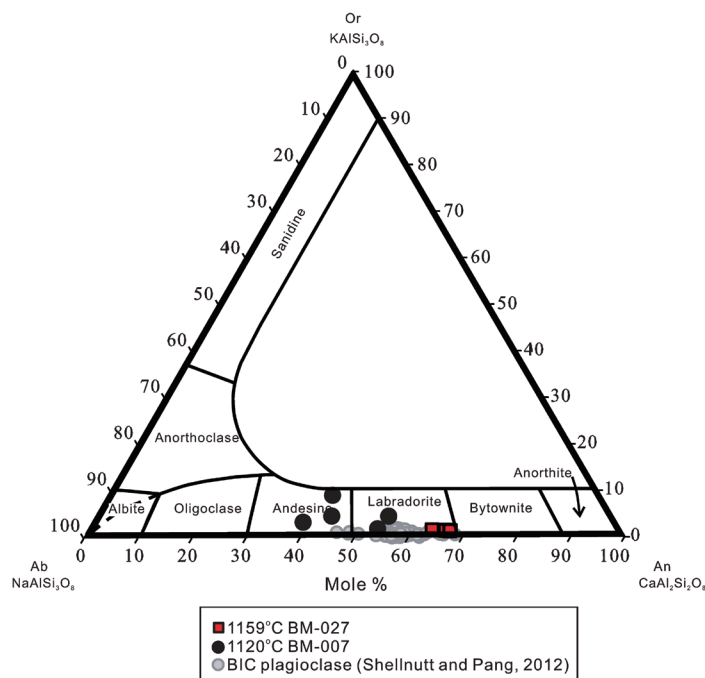

Fig. 5. Chemical classification of the experimental plagioclase in comparison to the plagioclase from the Baima layered gabbro.

Table 5. Average compositions of the plagioclase.

Sample	BM-027	s.d.	BM-007	s.d.
Temp. (°C)	1159	(3)	1125	(6)
SiO_2 (wt%)	51.85	0.37	55.77	1.90.
TiO_2	0.18	0.03	0.19	0.16
Al_2O_3	26.86	0.32	26.62	1.43
FeO	2.53	0.05	0.95	0.51
CaO	12.85	0.20	8.92	1.70
Na_2O	3.91	0.18	5.45	0.91
K_2O	0.24	0.01	0.64	0.31
Total	98.41		98.54	
Cations on the Basis of 8O				
Si	2.422	0.007	2.551	0.080
Ti	0.006	0.001	0.007	0.006
Al	1.478	0.013	1.435	0.074
Fe^{2+}	0.099	0.002	0.036	0.020
Ca	0.643	0.013	0.437	0.084
Na	0.354	0.013	0.483	0.080
K	0.014	0.001	0.038	0.018
Total	5.016		4.986	0.008
An	64	0.01	46	0.09
Ab	35	0.01	48	0.08
Or	1	0.0	4	0.02

Note: Minerals symbols: An = anorthite component; Ab = albite component; Or = orthoclase component. s.d. = standard deviation. Number in parenthesis is the total number of analysis.

Table 6. Average compositions of the glass and the Baima enclaves.

Sample	BM-023	s.d.	BM-005	s.d.	BM-026	s.d.	BM-027	s.d.	BM-007	s.d.	BM-1	BM-2	BM-4	BM-5
Temp. (°C)	1310	(74)	1300	(73)	1180	(6)	1159	(7)	1125	(4)				
SiO_2 (wt%)	45.66	0.26	46.61	0.37	51.47	0.22	53.59	0.78	57.58	0.39	58.12	62.94	60.08	57.20
TiO_2	4.01	0.10	3.98	0.12	2.91	0.12	2.54	0.32	2.04	0.22	1.46	0.77	1.03	1.80
Al_2O_3	12.34	0.28	12.56	0.23	13.90	0.19	13.74	1.16	15.14	0.46	16.19	16.98	16.36	14.18
Cr_2O_3			0.01	0.02	-	-	-	-	0.01	0.01				
FeOt	14.67	0.19	14.41	0.20	7.16	0.23	6.32	0.29	4.81	0.33	5.44	3.81	4.84	7.19
MnO	0.20	0.04	0.20	0.04	0.20	0.04	0.19	0.05	0.14	0.03	0.22	0.19	0.22	0.37
MgO	6.07	0.08	6.06	0.09	5.88	0.11	5.25	0.79	3.83	0.47	2.45	0.84	1.79	2.61
CaO	9.77	0.10	9.87	0.12	10.45	0.18	9.49	1.00	6.10	0.60	3.28	1.70	3.04	3.17
Na_2O	3.46	0.07	3.31	0.07	3.84	0.06	4.36	0.37	4.18	0.27	7.17	7.52	7.38	6.59
K_2O	1.17	0.03	1.16	0.03	1.38	0.03	1.69	0.13	2.84	0.32	3.88	4.66	4.22	4.16
Total	97.04		97.16		97.80		97.19		96.66		98.21	99.41	98.96	97.27
Mg#	42		43		59		60		59		44	28	40	39

Note: Enclave data from Shellnutt et al. (2010). FeOt of the Baima enclaves is calculated from Fe_2O_3t ($FeOt = 0.8998 \times Fe_2O_3t$).
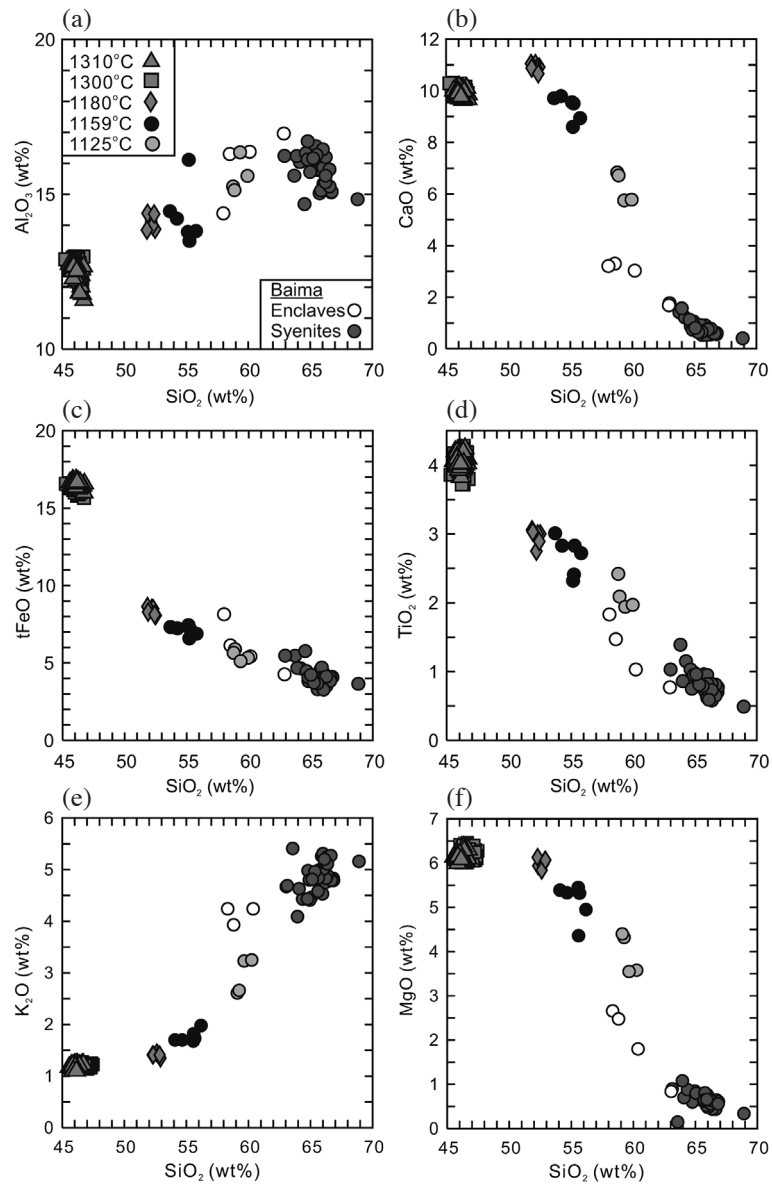
Fig. 6. Major element compositions of the glass from each run at low pressure. All data normalized to 100%. Baima syenite and enclave data from Shellnutt et al. (2009, 2010).

Table 7. Average whole rock trace elemental compositions of the glass.

| Sample	GS04-026	BM-023	s.d.	BM-005	s.d.	BM-026	s.d.	BM-027	s.d.	BM-007	s.d.
Temp. (°C)		1310	(9)	1300	(3)	1180	(2)	1159	(2)	1125	(3)
Ca (wt%)	10.16	9.70	0.05	9.79	0.07	10.65	0.25	9.36	0.19	6.67	1.53
Sc (ppm)	33	30.6	0.4	30.9	0.4	24.6	1.3	22.1	1.6	15.1	1.4
Cr	26	26.1	4.3	22.1	0.3	4.2	0.2	3.8	0.3	10.7	4.6
Ni	61	54.8	0.9	51.4	1.1	21.7	0.6	16.1	0.6	22.1	12.1
Rb	62	69.4	1.3	68.0	1.2	80.8	2.7	93.9	6.1	89.4	35.3
Sr	401	429	6.8	423	6.2	507	24.1	509	5.4	453	231
Y	26	25.8	0.7	26.0	0.5	28.5	1.3	31.7	0.3	24.3	10.0
Zr	165	173	5.9	174	3.2	194	24.9	215	34.2	152	119
Nb	21	24.2	0.6	23.5	0.2	28.4	2.0	29.0	0.2	21.9	10.1
Ba	310	321	7.7	313	6.7	369	19.5	422	11.2	405	112
La	24.5	24.5	0.7	23.9	0.5	28.1	1.5	31.4	0.7	27.4	10.3
Ce	54.2	55.0	1.3	53.0	1.2	63.7	2.8	70.1	1.7	60.3	23.2
Pr	7.2	7.4	0.2	7.1	0.2	8.5	0.4	9.4	0.3	7.7	3.1
Nd	30.5	31.8	0.8	30.6	0.7	36.1	2.0	40.1	0.7	31.9	12.9
Sm	6.8	6.9	0.2	6.6	0.2	7.7	0.5	8.7	0.5	6.4	2.5
Eu	2.2	2.2	0.1	2.2	0.1	2.5	0.1	2.8	0.1	2.3	0.7
Gd	6.0	6.3	0.2	6.3	0.1	7.0	0.2	7.6	0.2	5.8	2.5
Tb	1.0	0.9	0.0	0.9	0.0	1.0	0.1	1.1	0.0	0.8	0.3
Dy	5.5	5.4	0.1	5.4	0.2	5.9	0.3	6.6	0.3	5.1	1.9
Ho	1.0	1.0	0.0	1.0	0.0	1.1	0.1	1.3	0.0	0.9	0.3
Er	2.8	2.6	0.1	2.6	0.1	3.0	0.2	3.1	0.2	2.4	1.0
Tm	0.4	0.3	0.0	0.4	0.0	0.4	0.0	0.4	0.0	0.3	0.1
Yb	2.3	2.2	0.1	2.4	0.2	2.5	0.2	2.6	0.1	2.1	0.7
Lu	0.3	0.3	0.0	0.3	0.0	0.3	0.0	0.4	0.0	0.3	0.1
Hf	4.6	4.6	0.1	4.5	0.2	4.8	0.6	5.6	1.0	3.6	2.6
Ta	1.5	1.5	0.1	1.5	0.0	1.8	0.2	1.7	0.0	1.1	0.4
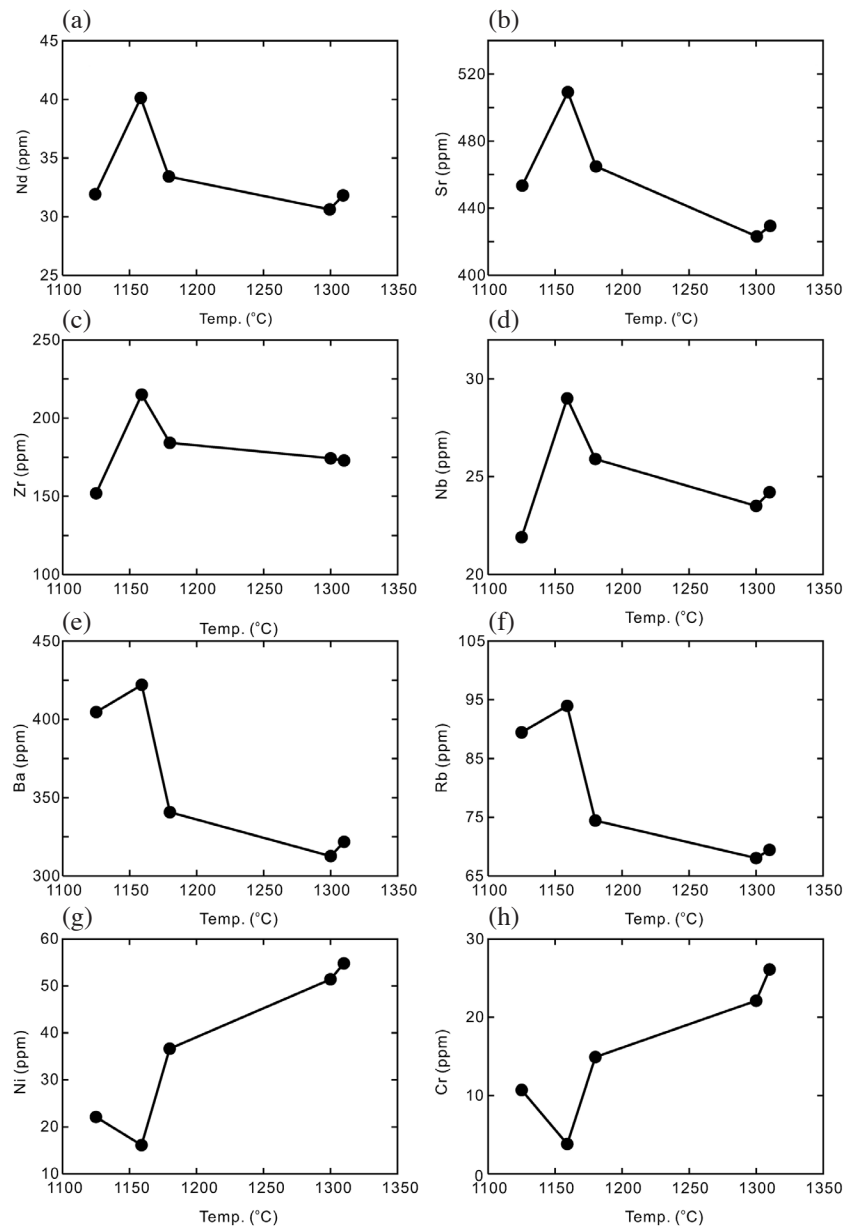
Fig. 7. Trace element compositions of the glass from each experiment at low pressure.

glasses are more similar in composition to the observed enclaves of the BIC syenitic unit (Fig. 6; Table 6). The microgranular enclaves are considered to be representative of the most primitive composition of the syenitic rocks before further differentiation to more silicic (SiO_2 > 62 wt%) compositions (Shellnutt et al. 2010). The Na_2O (lower; Table 6) and CaO (higher; Fig. 6) contents of the glass compositions are different from the enclaves but this is probably due to the anhydrous nature of the experiments as F, Cl, CO_2, and H_2O tend to increase the incompatibility of Na and rare earth elements and promote the crystallization of volatile-rich accessory minerals such as fluorite, bastnäsite, and titanite (Price et al. 1999; Scaillet and Macdonald 2004; Gysi and Williams-Jones 2015). The incompatible trace element evolution mirrors the major element composition. As the glass becomes more silicic, the incompatible (REE, Nb, Ta) trace elements become more enriched whereas the compatible (Ni, Cr, Sc) elements become depleted (Fig. 7).

The incompatible trace element evolution of the system is typified by Sr and Ba and resembles the geochemical modeling results of the Panxi gabbro-granitoid complexes (Fig. 8a). The geochemical models of the Panxi gabbro-granitoid complexes show that both Sr and Ba initially increase after early crystallization of titanomagnetite and mafic silicate minerals, and is followed by the decrease of Sr and increase of Ba due to the crystallization of plagioclase feldspar and then the decrease of both Sr and Ba due to the crystallization of alkali feldspar (Shellnutt et al. 2009, 2011; Shellnutt and Jahn 2010). A similar evolutionary path for Sr and Ba is shown in the low pressure models where Sr and Ba initially increase followed by a decrease in Sr and increase Ba (Fig. 8b). The two data points for the 1125°C experiment have very different compositions and thus it is difficult to reconcile their individual importance. We view the low Sr-Ba composition (Sr = ~260 ppm; Ba

= ~300 ppm) as anomalous as there is no indication of alkali feldspar crystallization in the system but there is no analytical reason to reject the data and therefore it may be meaningful. The similarity between the Sr-Ba experimental models and the geochemical models is supportive of the interpretation that the Baima syenite is derived from a parental magma similar to 'high-Ti' Emeishan basalt.

6.2 Implications for the Genesis of the Baima Oxide-Bearing Layered Gabbroic Intrusion

The Baima layered gabbroic intrusion is chiefly comprised of cumulus olivine, clinopyroxene, and plagioclase with interstitial Fe-Ti oxide and sulphide minerals. The oxide minerals periodically form thick ore-layers with the thickest layer near the base of the intrusion (Pang et al. 2010). Also, there is a distinct apatite-rich zone in the upper parts of the intrusion (Chen 1990; Shellnutt et al. 2009; Shellnutt and Pang 2012; Zhang et al. 2012; Chen et al. 2014; Liu et al. 2014a). It is interpreted that the Baima layered gabbroic intrusion and oxide deposit represent the solid residual portion of the parental magma or magmas that formed the Baima syenite (Yang et al. 1997; Shellnutt et al. 2009, 2011; Shellnutt and Pang 2012; Zhang et al. 2012). Therefore, if the modeled residual glass composition can replicate the observed Baima syenite microgranular enclaves then it is possible that the residual solid component may be able to shed light on the formation, textures, and structures observed in the layered gabbroic unit.

The composition of the Ti-rich magnetite is similar to the measured compositions from the Baima layered gabbro and the theorized primary oxide composition suggested by Shellnutt and Pang (2012). The compositions of the pyroxene and plagioclase are compared to the compositions analyzed from BIC layered gabbro in Figs. 4 and 5. The
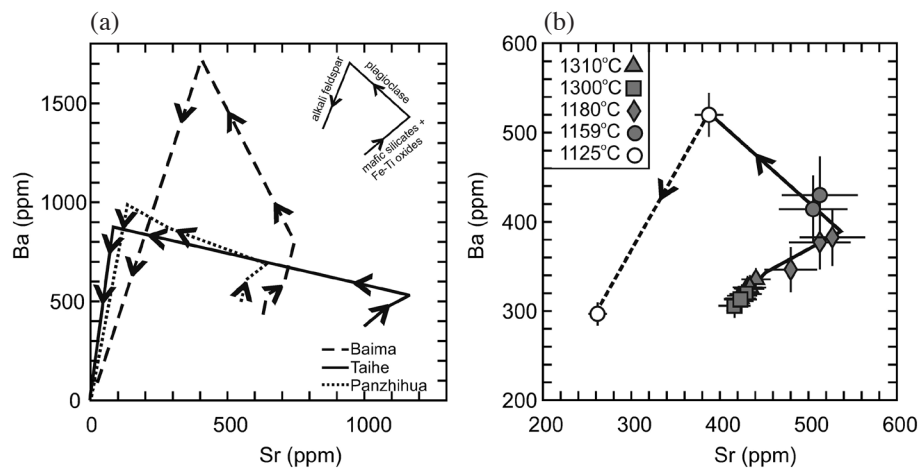

Fig. 8. (a) Geochemical models of Sr versus Ba evolution in the Baima, Panzhihua, and Taihe complexes (Shellnutt et al. 2009, 2010, 2011). (b) Experimental trend of Sr and Ba of the glass compositions. The dashed line connecting the low temperature compositions indicates an uncertain pathway (see text for details).

clinopyroxene and plagioclase crystals have similar compositions as those observed in the BIC gabbros. Specifically, the compositional range of the modeled clinopyroxene at 1180 and 1159°C overlap with the clinopyroxene from the gabbros whereas the lower temperature (1125°C) crystals tend to be more Fe-rich. The synthesized plagioclase, at all temperatures, is indistinguishable from the plagioclase of the gabbro (Fig. 5).

The early crystallization of titanomagnetite in the experiments is interesting as it may explain two important aspects of the layered gabbro. Firstly, early titanomagnetite crystallization explains the position of the oxide deposits within the lower parts of the layered gabbro. Moreover, it is possible that each Fe-Ti-rich horizon could represent an injection of a new batch of magma and the beginning of a new crystallization sequence as there is evidence for magma recharge in the system (Chen 1990; Shellnutt and Pang 2012; Zhang et al. 2012; Liu et al. 2014a). Secondly, mineral textures observed in the gabbro where silicate minerals and/or melt are enclosed by titanomagnetite and vice versa are replicated (Fig. 9). The application of QUIlF on the ilmenite-magnetite pairs of the lowest temperature runs indicates the relative oxidation state was above the FMQ buffer and ranges from ΔFMQ +0.3 to +1 or approximately equal to the Ni-NiO buffer (Andersen et al. 1993). The relative oxidation state estimate is within the range interpreted for the BIC system (Shellnutt et al. 2009, 2011; Zhang et al. 2012; Song et al. 2013).

6.3 Limitations of the Interpretations

The results of the experiments appear to replicate many textural, mineralogical, and chemical aspects of the BIC layered gabbroic and silicic units but there are limitations. Chiefly among the limitations is the verisimilitude of a small-scale experiment (< 1 gram) and relating it to a large-scale intrusion (≈100 km³). Although we selected a parental magma that is considered to be similar to the BIC system, the precise composition remains uncertain and it may have developed under polybaric conditions. Volatiles in the magma system are not constrained during the experiment but they are likely to play role as biotite and brown-hornblende are observed within the layered gabbro and magmatic fluorite is observed in the syenite.

The absence of olivine in the modeled crystallization sequence is an issue as the Baima layered gabbro contains olivine at various levels. However, sample GS04-026 does not contain olivine and thus its absence in the experiment is expected (Shellnutt et al. 2008). Moreover, sample GS04-026 probably experienced fractionation of olivine before emplacement (i.e., polybaric crystallization) as it is more evolved than a primary liquid (Herzberg and Asimow 2008; Shellnutt and Pham 2018). In the lower layers of the gabbro there is abundant olivine but the amount decreases at higher positions within the stratigraphy (Chen 1990; Shellnutt et al. 2009; Shellnutt and Pang 2012). It is very likely that the initial parental magma of the Baima gabbro was
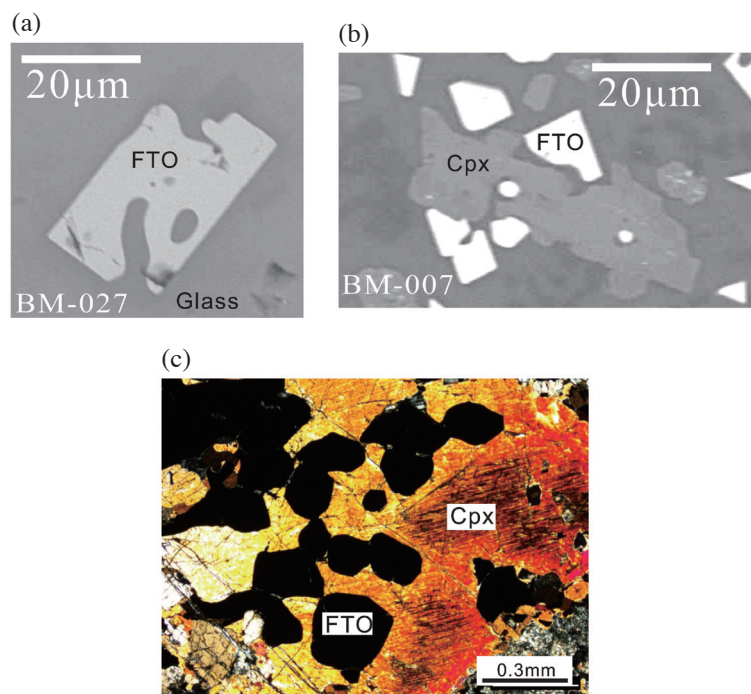

Fig. 9. (a) Iron-titanium oxide (FTO) mineral (Ti-magnetite) enclosing glass (Gl). (b) Clinopyroxene (Cpx) phenocryst enclosing Fe-Ti oxide (FTO) minerals. (c) Crossed polar photomicrograph of Ti-rich magnetite enclosed within clinopyroxene (Cpx) from the Panzhihua layered gabbro (courtesy of Kwan-Nang Pang).

more primitive or closer to a primary liquid composition than GS04-026. Therefore, it is possible that subsequent injections of new magma batches, as delineated by mineral chemistry changes and oxide-rich layers, may have been less primitive and therefore crystallized less olivine. Consequently, the experiment may be a better example of the conditions and magma composition of the upper gabbro zone as it is comprised of clinopyroxene, plagioclase, ilmenite, and magnetite with little to no olivine. In spite of the limitations, the experimental results indicate that the BIC gabbro, syenite, and oxide deposit can be derived from a common parental magma similar to high-Ti Emeishan basalt.

6.4 Role of Silicate Immiscibility and Carbonate Fluxing in the Formation of the BIC

Recent studies have suggested that some of the Panxi oxide-ore deposits may be, at least partially, formed by silicate-liquid immiscibility and/or carbonate fluxing (Zhou et al. 2005, 2013; Ganino et al. 2008, 2013a, b; Liu et al. 2014a, 2016). The extent of silicate-liquid immiscibility vis-à-vis a large scale or small scale process is uncertain as the evidence for immiscibility is based on mineral or melt inclusion studies whereas carbonate fluxing is based on the contact relationship between the parental magma of the Panzhihua intrusion and marble country rock.

Experimental studies show that tholeiitic and alkalic basaltic liquids may enter conditions of silicate-liquid immiscibility after a period of crystal fractionation and produce an Fe-rich silicate liquid and a Si-rich silicate liquid (Philpotts 1976, 1982; Watson 1976; Naslund 1983; Veksler et al. 2007, 2008; Veksler 2009; Shellnutt et al. 2013). The bulk composition of the Si-rich silicate liquid is similar to granitic rocks in general whereas the Fe-rich silicate liquid resembles a mafic-ultramafic rock. The evidence for silicate immiscibility within the Panxi intrusions is based on observations and chemistry from mineral and melt inclusions and experimental results (Wang et al. 2013; Liu et al. 2014a, 2016; Hou and Veksler 2015; Xing et al. 2017). Although the evidence for small-scale silicate immiscibility is compelling, it is less clear that large-scale silicate immiscibility occurred. Specifically, there are a number of observations within the Baima layered gabbroic intrusion that cannot be easily explained by immiscibility and include: (1) systematic compositional evolution within the layered gabbro, (2) distribution of the incompatible elements in minerals or whole rock, and (3) the absence of a contemporaneous silicic plutonic body that is depleted in incompatible elements (Watson 1976; Veksler et al. 2006).

It appears that multiple magma pulses and internal redistribution occurred within the Baima system as the mineral composition trend is periodically interrupted but there is a broad systematic evolution from bottom to top where the base of the intrusion has more primitive compositions (Fo ≈

75; An ≈ 65) and the upper portions are more evolved (Fo ≈ 60; An ≈ 50) (Chen 1990; Shellnutt and Pang 2012; Zhang et al. 2012; Liu et al. 2014a). It is possible that the mineral compositional evolution may be due to injection of progressively less mafic basalts thereby creating the appearance of a systematic evolution but there is a distinct association between the composition of the minerals and their stratigraphic position. Assuming silicate-liquid immiscibility is not disturbed by the injection of new magma batches, there appears to be a dearth of highly calcic (An > 80) plagioclase that would be expected to crystallize from the Fe-rich silicate liquid. If large-scale silicate immiscibility occurred then there should be layers or even a periodic discovery of coarse grained non-cumulus calcic plagioclase because the Fe-rich immiscible liquid is alkali-poor and relatively Ca-rich. To date, significant amounts of coarse grained, non-cumulus Ca-rich feldspar have yet to be identified by detailed mineralogical investigations (Chen 1990; Shellnutt and Pang 2012; Zhang et al. 2012; Liu et al. 2014a).

The results of trace element partitioning between the immiscible silicate melts by Watson (1976) and Veksler et al. (2006) showed that nearly all incompatible elements (Zr, Hf, Ti, Nb, Ta, and REEs) partition into the Fe-rich endmember due to its low polymerization and only Rb and Cs appear to prefer the Si-rich melt. The bulk rock compositions from different units of the Baima layered gabbro do not show unusually high concentrations of incompatible elements as most incompatible trace elements (Y, Zr, Hf, Nb, Ta, and REEs) have concentrations < 10 ppm (Shellnutt et al. 2009; Zhang et al. 2012). If the partition experiments of Watson (1976) and Veksler et al. (2006) are correct and that the thick oxide deposits formed due to immiscibility, then there should be zones or layers of equal volume to the oxiderich layers that contain the incompatible elements. At the moment, enriched zones or layers of REEs, Y, Ta, Hf, Zr, Nb have yet to be identified within the Baima layered gabbro.

Thus far, a large-scale plutonic body representing the Si-rich immiscible end-member has yet to be identified although Liu et al. (2016) suggest it could be the fayalite-bearing syenite (Huangcao pluton) to the west of the Baima layered gabbro. The Huangcao syenite contains fayalite, ferrohedenbergite, alkali feldspar, quartz, apatite, ferrosilite, and Fe-Ti oxides (ilmenite and magnetite) and is considered to be formed by partial melting of underplated mafic rocks that are related to the Emeishan large igneous province (Shellnutt and Zhou 2008; Shellnutt and Iizuka 2012). The Huangcao pluton is probably not representative of the Si-rich immiscible melt because it demonstrates enrichment of Ba, Zr, Ta, Nb, and REE and depletion of Cs relative to the Baima layered gabbro and also has a positive chondrite normalized Eu-anomaly (Eu/Eu* > 1.1). If the Baima parental magma is required to undergo "prolonged fractional crystallization of plagioclase" before immiscibility then the resultant liquids should have either a neutral Eu-anomaly

(i.e., Eu/Eu* ≈ 1) or, more likely, have a negative Eu-anomaly (Liu et al. 2016). Moreover, Fe-rich silicate minerals are a common feature of many ferroan (A-type) granites (Frost and Frost 1997, 2011; Civetta et al. 1998; Frost et al. 2001; Melluso et al. 2008).

An interesting result from the experiments of this study is the formation of inclusion textures of oxide minerals in clinopyroxene and vice versa (Fig. 9). Inclusion textures of oxides within silicates observed in the Baima layered gabbro are interpreted to be evidence of silicate immiscibility (Liu et al. 2014b, 2016). Based on our results, the inclusion textures form as a consequence of crystallization. Correspondingly, the early crystallization of oxide minerals in this study is likely directly related to the parental magma composition and relative oxidation state suggesting that some 'high-Ti' Emeishan mafic magmas are at or close to Fe-Ti saturation when they are emplaced and thus will preferentially crystallize titanomagnetite immediately upon cooling rather than silicate minerals. The early crystallization of titanomagnetite will therefore increase the likelihood that it will be enclosed by a silicate mineral.

Carbonate country rock assimilation, as observed by carbonate xenoliths within the Panzhihua layered intrusion, is suggested as a process for increasing the relative oxidation state of the Panxi oxide deposits and thereby inducing en masse crystallization of Fe-Ti oxide minerals (Ganino et al. 2008, 2013a, b; Bai et al. 2012; Pang et al. 2013; Tang et al. 2017). It is very likely that there was an interaction between carbonate country rocks and the magma that formed the Panzhihua complex as there are carbonate xenoliths found within the lower units of the gabbro. However, carbonate xenoliths are absent within in the Baima complex (Tang et al. 2017). It seems, from the experimental results, that carbonate assimilation may not be required to induce oxide mineral crystallization because the first mineral to crystallize from high-Ti Emeishan basalt is expected to be titanomagnetite at a relative oxidation state of ΔFMQ +1. The average relative oxidation state of all Emeishan basalt using the method of Kress and Carmichael (1991) is ΔFMQ +0.1 (total range ΔFMQ -1.0 to +1.3) (Shellnutt and Iizuka 2012). Furthermore, the Sr isotopes of the Panxi layered gabbros do not appear to be highly enriched within the main body of the intrusion and suggests that contamination was probably a localized process around the contact margins (Shellnutt et al. 2009, 2011; Howarth and Prevec 2013). Therefore, assimilation of carbonate country rocks may be unnecessary to form the oxide deposits.

7. CONCLUDING REMARKS

The experiments resulted in a number of observations including:
(1) The crystallization sequence in the experiments is: Fe-Ti oxide (1303°C); clinopyroxene (1184°C); and plagio-clase (1162°C).
(2) The compositions of the synthesized clinopyroxene and plagioclase are similar to the mineral compositions from the BIC layered gabbro.
(3) The residual glass compositions from the low temperature experiments are similar to the known composition of the Baima syenitic enclaves.
(4) Enclosure textures of oxide and silicate minerals in the gabbroic rocks are replicated in this study.
From the experimental observations we conclude that:
(1) The low pressure experiments were able to replicate the silicic enclave composition of the Baima syenitic unit, and the plagioclase and clinopyroxene compositions of the Baima layered gabbros. Therefore, it is possible that the layered gabbroic intrusion, oxide-ore deposit, and syenitic pluton of the BIC are a cogenetic complex that formed at low pressure.
(2) The Fe-Ti oxide deposits of the Baima layered gabbroic intrusion and possibly the Panzhihua and Taihe intrusions may have formed *in situ* and early during the crystallization of a basaltic parental magma. New batches of isotopically similar basaltic magmas were likely repeatedly injected into the same magma chamber and formed new Fe-Ti oxide horizons. Therefore, the presence of an oxide-dominant horizon within the layered gabbroic units may indicate a new magma pulse.

REFERENCES

Ali, J. R., G. M. Thompson, M.-F. Zhou, and X. Song, 2005: Emeishan large igneous province, SW China. *Lithos*, **79**, 475-489, doi: 10.1016/j.lithos.2004.09.013. [Link]

Andersen, D. J., D. H. Lindsley, and P. M. Davidson, 1993: QUIlF: A Pascal program to assess equilibria among Fe-Mg-Mn-Ti oxides, pyroxenes, olivine, and quartz. *Comput. Geosci.*, **19**, 1333-1350, doi: 10.1016/0098-3004(93)90033-2. [Link]

Bai, Z.-J., H. Zhong, A. J. Naldrett, W.-G. Zhu, and G.-W. Xu, 2012: Whole-rock and mineral composition constraints on the genesis of the giant Hongge Fe-Ti-V oxide deposit in the Emeishan large igneous province, southwest China. *Econ. Geol.*, **107**, 507-524, doi: 10.2113/econgeo.107.3.507. [Link]

Bai, Z.-J., H. Zhong, C. Li, W.-G. Zhu, D.-F. He, and L. Qi, 2014: Contrasting parental magma compositions for

the Hongge and Panzhihua magmatic Fe-Ti-V oxide deposits, Emeishan large igneous province, SW China. *Econ. Geol.*, **109**, 1763-1785, doi: 10.2113/econgeo.109.6.1763. [Link]

Bai, Z.-J., H. Zhong, C. Li, W.-G. Zhu, and W.-J. Hu, 2016: Association of cumulus apatite with compositionally unusual olivine and plagioclase in the Taihe Fe-Ti oxide ore-bearing layered mafic-ultramafic intrusion: Petrogenetic significance and implications for ore genesis. *Am. Mineral.*, **101**, 2168-2175, doi: 10.2138/am-2016-5577. [Link]

Bonin, B., 2007: A-type granites and related rocks: Evolution of a concept, problems and prospects. *Lithos*, **97**, 1-29, doi: 10.1016/j.lithos.2006.12.007. [Link]

Cawthorn, R. G., 1996: Layered Intrusions, Developments in Petrology, Vol. 15, Elsevier, Netherlands, 530 pp.

Charlier, B., O. Namur, R. Latypov, and C. Tegner, 2015: Layered Intrusions, Springer Netherlands, 748 pp, doi: 10.1007/978-94-017-9652-1. [Link]

Chen, F., 1990: Petrologic study on Baima ore-bearing layered mafic-ultramafic intrusion. *Acta Petrologica Sinica*, **4**, 12-25. (in Chinese)

Chen, L.-M., X.-Y. Song, X.-K. Zhu, X.-Q. Zhang, S.-Y. Yu, and J.-N. Yi, 2014: Iron isotope fractionation during crystallization and sub-solidus re-equilibration: Constraints from the Baima mafic layered intrusion, SW China. *Chem. Geol.*, **380**, 97-109, doi: 10.1016/j.chemgeo.2014.04.020. [Link]

Chen, L.-M., X.-Y. Song, R.-Z. Hu, S.-Y. Yu, H.-L. He, Z.-H. Dai, Y.-W. She, and W. Xie, 2017: Controls on trace-element partitioning among co-crystallizing minerals: Evidence from the Panzhihua layered intrusion, SW China. *Am. Mineral.*, **102**, 1006-1020, doi: 10.2138/am-2017-5804. [Link]

Civetta, L., M. D'Antonio, G. Orsi, and G. R. Tilton, 1998: The geochemistry of volcanic rocks from Pantelleria Island, Sicily Channel: Petrogenesis and characteristics of the mantle source region. *J. Petrol.*, **39**, 1453-1491, doi: 10.1093/petroj/39.8.1453. [Link]

Duchesne, J. C., 1999: Fe-Ti deposits in Rogaland anorthosites (South Norway): Geochemical characteristics and problems of interpretation. *Miner. Depos.*, **34**, 182-198, doi: 10.1007/s001260050195. [Link]

Frost, B. R., C. G. Barnes, W. J. Collins, R. J. Arculus, D. J. Ellis, and C. D. Frost, 2001: A geochemical classification for granitic rocks. *J. Petrol.*, **42**, 2033-2048.

Frost, C. D. and B. R. Frost, 1997: Reduced rapakivi-type granites: The tholeiite connection. *Geology*, **25**, 647-650, doi: 10.1130/0091-7613(1997)025<0647:RRTGTT>2.3.CO;2. [Link]

Frost, C. D. and B. R. Frost, 2011: On ferroan (A-type) granitoids: Their compositional variability and modes of origin. *J. Petrol.*, **52**, 39-53, doi: 10.1093/petrology/egq070. [Link]

Ganino, C., N. T. Arndt, M.-F. Zhou, F. Gaillard, and C. Chauvel, 2008: Interaction of magma with sedimentary wall rock and magnetite ore genesis in the Panzhihua mafic intrusion, SW China. *Miner. Depos.*, **43**, 677-694, doi: 10.1007/s00126-008-0191-5. [Link]

Ganino, C., C. Harris, N. T. Arndt, S. A. Prevec, and G. H. Howarth, 2013a: Assimilation of carbonate country rock by the parent magma of the Panzhihua Fe-Ti-V deposit (SW China): Evidence from stable isotopes. *Geosci. Front.*, **4**, 547-554, doi: 10.1016/j.gsf.2012.12.006. [Link]

Ganino, C., N. T. Arndt, C. Chauvel, A. Jean, and C. Athurion, 2013b: Melting of carbonate wall rocks and formation of the heterogeneous aureole of the Panzhihua intrusion, China. *Geosci. Front.*, **4**, 535-546, doi: 10.1016/j.gsf.2013.01.012. [Link]

Gysi, A. P. and A. E. Williams-Jones, 2015: The thermodynamic properties of bastnäsite-(Ce) and parisite-(Ce). *Chem. Geol.*, **392**, 87-101, doi: 10.1016/j.chemgeo.2014.11.001. [Link]

Herzberg, C. and P. D. Asimow, 2008: Petrology of some oceanic island basalts: PRIMELT2.XLS software for primary magma calculation. *Geochem. Geophys. Geosyst.*, **9**, Q09001, doi: 10.1029/2008GC002057. [Link]

Hou, T. and I. V. Veksler, 2015: Experimental confirmation of high-temperature silicate liquid immiscibility in multicomponent ferrobasaltic systems. *Am. Mineral.*, **100**, 1304-1307, doi: 10.2138/am-2015-5285. [Link]

Howarth, G. H. and S. A. Prevec, 2013: Trace element, PGE, and Sr-Nd isotope geochemistry of the Panzhihua mafic layered intrusion, SW China: Constraints on ore-forming processes and evolution of parent magma at depth in a plumbing-system. *Geochim. Cosmochim. Acta*, **120**, 459-478, doi: 10.1016/j.gca.2013.06.019. [Link]

Iyer, H. M., 1984: Geophysical evidence for the locations, shapes and sizes, and internal structures of magma chambers beneath regions of Quaternary volcanism. *Phil. Trans. Roy. Soc. Lond. Math. Phys. Sci.*, **310**, 473-510, doi: 10.1098/rsta.1984.0005. [Link]

Kress, V. C. and I. S. E. Carmichael, 1991: The compressibility of silicate liquids containing Fe_2O_3 and the effect of composition, temperature, oxygen fugacity and pressure on their redox states. *Contrib. Mineral. Petrol.*, **108**, 82-92, doi: 10.1007/bf00307328. [Link]

Lee, C. A., 1996: A review of mineralization in the Bushveld Complex and some other layered intrusions. In: Cawthorn, R. G. (Ed.), Layered Intrusions, Developments in Petrology, Vol. 15, Elsevier, Netherlands, 103-145, doi: 10.1016/S0167-2894(96)80006-6. [Link]

Liu, P.-P., M.-F. Zhou, C. Y. Wang, C.-M. Xing, and J.-F. Gao, 2014a: Open magma chamber processes in the formation of the Permian Baima mafic-ultramafic layered intrusion, SW China. *Lithos*, **184-187**, 194-208,

doi: 10.1016/j.lithos.2013.10.028. [Link]

Liu, P.-P., M.-F. Zhou, W. T. Chen, M. Boone, and V. Cnudde, 2014b: Using multiphase solid inclusions to constrain the origin of the Baima Fe-Ti-(V) oxide deposit, SW China. *J. Petrol.*, **55**, 951-976, doi: 10.1093/petrology/egu012. [Link]

Liu, P.-P., M.-F. Zhou, Z. Ren, C. Y. Wang, and K. Wang, 2016: Immiscible Fe- and Si-rich silicate melts in plagioclase from the Baima mafic intrusion (SW China): Implications for the origin of bi-modal igneous suites in large igneous provinces. *J. Asian Earth Sci.*, **127**, 211-230, doi: 10.1016/j.jseaes.2016.04.026. [Link]

Melluso, L., C. Cucciniello, C. M. Petrone, M. Lustrino, V. Morra, M. Tiepolo, and L. Vasconcelos, 2008: Petrology of Karoo volcanic rocks in the southern Lebombo monocline, Mozambique. *J. Afr. Earth Sci.*, **52**, 139-151, doi: 10.1016/j.jafrearsci.2008.06.002. [Link]

Mondal, S. K. and W. L. Griffin, 2017: Processes and Ore Deposits of Ultramafic-Mafic Magmas through Space and Time, Elsevier, 382 pp.

Murru, M., C. Montuori, M. Wyss, and E. Privitera, 1999: The locations of magma chambers at Mt. Etna, Italy, mapped by b-values. *Geophys. Res. Lett.*, **26**, 2553-2556, doi: 10.1029/1999gl900568. [Link]

Naslund, H. R., 1983: The effect of oxygen fugacity on liquid immiscibility in iron-bearing silicate melts. *Am. J. Sci.*, **283**, 1034-1059, doi: 10.2475/ajs.283.10.1034. [Link]

Pang, K.-N. and J. G. Shellnutt, 2017: Magmatic sulfide and Fe-Ti oxide deposits associated with mafic-ultramafic intrusions in China. In: Mondal, S. K. and W. L. Griffin (Eds.), Processes and Ore Deposits of Ultramafic-Mafic Magmas through Space and Time, Elsevier, 239-267.

Pang, K.-N., C. Li, M.-F. Zhou, and E. M. Ripley, 2008a: Abundant Fe-Ti oxide inclusions in olivine from the Panzhihua and Hongge layered intrusions, SW China: Evidence for early saturation of Fe-Ti oxides in ferrobasaltic magma. *Contrib. Mineral. Petrol.*, **156**, 307-321, doi: 10.1007/s00410-008-0287-z. [Link]

Pang, K.-N., M.-F. Zhou, D. Lindsley, D. Zhao, and J. Malpas, 2008b: Origin of Fe-Ti oxide ores in mafic intrusions: Evidence from the Panzhihua intrusion, SW China. *J. Petrol.*, **49**, 295-313, doi: 10.1093/petrology/egm082. [Link]

Pang, K.-N., C. Li, M.-F. Zhou, and E. M. Ripley, 2009: Mineral compositional constraints on petrogenesis and oxide ore genesis of the late Permian Panzhihua layered gabbroic intrusion, SW China. *Lithos*, **110**, 199-214, doi: 10.1016/j.lithos.2009.01.007. [Link]

Pang, K.-N., M.-F. Zhou, L. Qi, J. G. Shellnutt, C. Y. Wang, and D. Zhao, 2010: Flood basalt-related Fe-Ti oxide deposits in the Emeishan large igneous province, SW China. *Lithos*, **119**, 123-136, doi: 10.1016/j.lith-

os.2010.06.003. [Link]

Pang, K.-N., N. Arndt, H. Svensen, S. Planke, A. Polozov, S. Polteau, Y. Iizuka, and S.-L. Chung, 2013: A petrologic, geochemical and Sr-Nd isotopic study on contact metamorphism and degassing of Devonian evaporites in the Norilsk aureoles, Siberia. *Contrib. Mineral. Petrol.*, **165**, 683-704, doi: 10.1007/s00410-012-0830-9. [Link]

Pêcher, A., N. Arndt, A. Jean, A. Bauville, C. Ganino, and C. Athurion, 2013: Structure of the Panzhihua intrusion and its Fe-Ti-V deposit, China. *Geosci. Front.*, **4**, 571-581, doi: 10.1016/j.gsf.2013.02.004. [Link]

Philpotts, A. R., 1967: Origin of certain iron-titanium oxide and apatite rocks. *Econ. Geol.*, **62**, 303-315, doi: 10.2113/gsecongeo.62.3.303. [Link]

Philpotts, A. R., 1976: Silicate liquid immiscibility: Its probable extent and petrogenetic significance. *Am. J. Sci.*, **276**, 1147-1177, doi: 10.2475/ajs.276.9.1147. [Link]

Philpotts, A. R., 1982: Compositions of immiscible liquids in volcanic rocks. *Contrib. Mineral. Petrol.*, **80**, 201-218, doi: 10.1007/bf00371350. [Link]

Price, J. D., J. P. Hogan, M. C. Gilbert, D. London, and G. B. Morgan VI, 1999: Experimental study of titanite-fluorite equilibria in the A-type Mount Scott granite: Implications for assessing F contents of felsic magma. *Geology*, **27**, 951-954, doi: 10.1130/0091-7613(1999)027<0951:ESOTFE>2.3. CO;2. [Link]

Scaillet, B. and R. Macdonald, 2004: Fluorite stability in silicic magmas. *Contrib. Mineral. Petrol.*, **147**, 319-329, doi: 10.1007/s00410-004-0559-1. [Link]

She, Y.-W., S.-Y. Yu, X.-Y. Song, L.-M. Chen, W.-Q. Zheng, and Y. Luan, 2014: The formation of P-rich Fe-Ti oxide ore layers in the Taihe layered intrusion, SW China: Implications for magma-plumbing system process. *Ore Geol. Rev.*, **57**, 539-559, doi: 10.1016/j.oregeorev.2013.07.007. [Link]

Shellnutt, J. G., 2014: The Emeishan large igneous province: A synthesis. *Geosci. Front.*, **5**, 369-394, doi: 10.1016/j.gsf.2013.07.003. [Link]

Shellnutt, J. G. and Y. Iizuka, 2011: Mineralogy from three peralkaline granitic plutons of the Late Permian Emeishan large igneous province (SW China): Evidence for contrasting magmatic conditions of A-type granitoids. *Eur. J. Mineral.*, **23**, 45-61, doi: 10.1127/0935-1221/2010/0022-2073. [Link]

Shellnutt, J. G. and Y. Iizuka, 2012: Oxidation zonation within the Emeishan large igneous province: Evidence from mantle-derived syenitic plutons. *J. Asian Earth Sci.*, **54-55**, 31-40, doi: 10.1016/j.jseaes.2012.03.011. [Link]

Shellnutt, J. G. and B.-M. Jahn, 2010: Formation of the Late Permian Panzhihua plutonic-hypabyssal-volcanic igneous complex: Implications for the genesis of

Fe-Ti oxide deposits and A-type granites of SW China. *Earth Planet. Sci. Lett.*, **289**, 509-519, doi: 10.1016/j.epsl.2009.11.044. [Link]

Shellnutt, J. G. and K.-N. Pang, 2012: Petrogenetic implications of mineral chemical data for the Permian Baima igneous complex, SW China. *Mineral. Petrol.*, **106**, 75-88, doi: 10.1007/s00710-012-0217-7. [Link]

Shellnutt, J. G. and T. T. Pham, 2018: Mantle potential temperature estimates and primary melt compositions of the Low-Ti Emeishan flood basalt. *Front. Earth Sci.*, **6**, doi: 10.3389/feart.2018.00067. [Link]

Shellnutt, J. G. and M.-F. Zhou, 2007: Permian peralkaline, peraluminous and metaluminous A-type granites in the Panxi district, SW China: Their relationship to the Emeishan mantle plume. *Chem. Geol.*, **243**, 286-316, doi: 10.1016/j.chemgeo.2007.05.022. [Link]

Shellnutt, J. G. and M.-F. Zhou, 2008: Permian, rifting related fayalite syenite in the Panxi region, SW China. *Lithos*, **101**, 54-73, doi: 10.1016/j.lithos.2007.07.007. [Link]

Shellnutt, J. G., M.-F. Zhou, D.-P. Yan, and Y. Wang, 2008: Longevity of the Permian Emeishan mantle plume (SW China): 1 Ma, 8 Ma or 18 Ma? *Geol. Mag.*, **145**, 373-388, doi: 10.1017/S0016756808004524. [Link]

Shellnutt, J. G., M.-F. Zhou, and G. F. Zellmer, 2009: The role of Fe–Ti oxide crystallization in the formation of A-type granitoids with implications for the Daly gap: An example from the Permian Baima igneous complex, SW China. *Chem. Geol.*, **259**, 204-217, doi: 10.1016/j.chemgeo.2008.10.044. [Link]

Shellnutt, J. G., B.-M. Jahn, and J. Dostal, 2010: Elemental and Sr-Nd isotope geochemistry of microgranular enclaves from peralkaline A-type granitic plutons of the Emeishan large igneous province, SW China. *Lithos*, **119**, 34-46, doi: 10.1016/j.lithos.2010.07.011. [Link]

Shellnutt, J. G., K.-L. Wang, G. F. Zellmer, Y. Iizuka, B.-M. Jahn, K.-N. Pang, L. Qi, and M.-F. Zhou, 2011: Three Fe-Ti oxide ore-bearing gabbro-granitoid complexes in the Panxi region of the Permian Emeishan large igneous province, SW China. *Am. J. Sci.*, **311**, 773-812, doi: 10.2475/09.2011.02. [Link]

Shellnutt, J. G., S. W. Denyszyn, and R. Mundil, 2012: Precise age determination of mafic and felsic intrusive rocks from the Permian Emeishan large igneous province (SW China). *Gondwana Res.*, **22**, 118-126, doi: 10.1016/j.gr.2011.10.009. [Link]

Shellnutt, J. G., J. Dostal, and Y. Iizuka, 2013: Evidence of silicate immiscibility within flood basalts from the Central Atlantic Magmatic Province. *Geochem. Geophys. Geosyst.*, **14**, 4921-4935, doi: 10.1002/2013gc004977. [Link]

Shellnutt, J. G., G. S.-K. Ma, and L. Qi, 2015: Platinum-group elemental chemistry of the Baima and Taihe Fe-Ti oxide bearing gabbroic intrusions of the Emeishan large igneous province, SW China. *Geochemistry*, **75**, 35-49, doi: 10.1016/j.chemer.2014.06.002. [Link]

Song, X.-Y., M.-F. Zhou, R. R. Keays, Z.-M. Cao, M. Sun, and L. Qi, 2006: Geochemistry of the Emeishan flood basalts at Yangliuping, Sichuan, SW China: Implications for sulfide segregation. *Contrib. Mineral. Petrol.*, **152**, 53-74, doi: 10.1007/s00410-006-0094-3. [Link]

Song, X.-Y., H.-W. Qi, R.-Z. Hu, L.-M. Chen, S.-Y. Yu, and J.-F. Zhang, 2013: Formation of thick stratiform Fe-Ti oxide layers in layered intrusion and frequent replenishment of fractionated mafic magma: Evidence from the Panzhihua intrusion, SW China. *Geochem. Geophys. Geosyst.*, **14**, 712-732, doi: 10.1002/ggge.20068. [Link]

Tang, Q., C. Li, Y. Tao, E. M. Ripley, and F. Xiong, 2017: Association of Mg-rich olivine with magnetite as a result of brucite marble assimilation by basaltic magma in the Emeishan large igneous province, SW China. *J. Petrol.*, **58**, 699-714, doi: 10.1093/petrology/egx031. [Link]

Van Tongeren, J. A. and E. A. Mathez, 2012: Large-scale liquid immiscibility at the top of the Bushveld Complex, South Africa. *Geology*, **40**, 491-494, doi: 10.1130/g32980.1. [Link]

Veksler, I. V., 2009: Extreme iron enrichment and liquid immiscibility in mafic intrusions: Experimental evidence revisited. *Lithos*, **111**, 72-82, doi: 10.1016/j.lithos.2008.10.003. [Link]

Veksler, I. V., A. M. Dorfman, L. V. Danyushevsky, J. K. Jakobsen, and D. B. Dingwell, 2006: Immiscible silicate liquid partition coefficients: Implications for crystal-melt element partitioning and basalt petrogenesis. *Contrib. Mineral. Petrol.*, **152**, 685-702, doi: 10.1007/s00410-006-0127-y. [Link]

Veksler, I. V., A. M. Dorfman, A. A. Borisov, R. Wirth, and D. B. Dingwell, 2007: Liquid immiscibility and the evolution of basaltic magma. *J. Petrol.*, **48**, 2187-2210, doi: 10.1093/petrology/egm056. [Link]

Veksler, I. V., A. M. Dorfman, D. Rhede, R. Wirth, A. A. Borisov, and D. B. Dingwell, 2008: Liquid unmixing kinetics and the extent of immiscibility in the system K_2O-CaO-FeO-Al_2O_3-SiO_2. *Chem. Geol.*, **256**, 119-130, doi: 10.1016/j.chemgeo.2008.06.033. [Link]

Wager, L. R. and G. M. Brown, 1968: Layered Igneous Rocks, Oliver and Boyd, Edinburgh, 588 pp.

Wang, C. Y., M.-F. Zhou, and L. Qi, 2007: Permian flood basalts and mafic intrusions in the Jinping (SW China)–Song Da (northern Vietnam) district: Mantle sources, crustal contamination and sulfide segregation. *Chem. Geol.*, **243**, 317-343, doi: 10.1016/j.chemgeo.2007.05.017. [Link]

Wang, D. R., Y. M. Xie, Q. J. Wang, and Z. D. Tao, 1994: Geology of Guabang area. Map G-48-25-C, Panxi Geological Team, Geology and Mineral Resources

Bureau of Sichuan Province, 1:50000.

Wang, K., C. M. Xing, Z. Y. Ren, and Y. Wang, 2013: Liquid immiscibility in the Panzhihua mafic layered intrusion: Evidence from melt inclusions in apatite. *Acta Petrologica Sinica*, **29**, 3503-3518. (in Chinese)

Watson, E. B., 1976: Two-liquid partition coefficients: Experimental data and geochemical implications. *Contrib. Mineral. Petrol.*, **56**, 119-134, doi: 10.1007/bf00375424. [Link]

Xing, C.-M., C. Y. Wang, and W. Tan, 2017: Disequilibrium growth of olivine in mafic magmas revealed by phosphorus zoning patterns of olivine from mafic-ultramafic intrusions. *Earth Planet. Sci. Lett.*, **479**, 108-119, doi: 10.1016/j.epsl.2017.09.005. [Link]

Xiong, X. Y., Y. M. Xie, K. H. Nie, Z. Z. Kan, L. R. Ding, and J. Q. Guo, 1996: Geology of Miyi area. Map G-48-37-A, Geology and Mineral Resources Bureau of Sichuan Province, 1:50000.

Xu, Y., S.-L. Chung, B.-M. Jahn, and G. Wu, 2001: Petrologic and geochemical constraints on the petrogenesis of Permian-Triassic Emeishan flood basalts in southwestern China. *Lithos*, **58**, 145-168, doi: 10.1016/s0024-4937(01)00055-x. [Link]

Yang, R., W. Xu, and R. Liu, 1997: REE geochemistry of Baima complex in the Panxi rift belt. *Acta Mineralogica Sinica*, **17**, 71-77. (in Chinese)

Zhang, X.-Q., X.-Y. Song, L.-M. Chen, W. Xie, S.-Y. Yu, W.-Q. Zheng, Y.-F. Deng, J.-F. Zhang, and S.-G. Gui, 2012: Fractional crystallization and the formation of thick Fe-Ti-V oxide layers in the Baima layered intrusion, SW China. *Ore Geol. Rev.*, **49**, 96-108, doi: 10.1016/j.oregeorev.2012.09.003. [Link]

Zhang, Z., J. Mao, A. D. Saunders, Y. Ai, Y. Li, and L. Zhao, 2009: Petrogenetic modeling of three mafic-ultramafic layered intrusions in the Emeishan large igneous province, SW China, based on isotopic and bulk chemical constraints. *Lithos*, **113**, 369-392, doi: 10.1016/j.lithos.2009.04.023. [Link]

Zhong, H., X.-H. Zhou, M.-F. Zhou, M. Sun, and B.-G. Liu, 2002: Platinum-group element geochemistry of the Hongge Fe-V-Ti deposit in the Pan-Xi area, southwestern China. *Miner. Depos.*, **37**, 226-239, doi: 10.1007/s00126-001-0220-0. [Link]

Zhong, H., R.-Z. Hu, A. H. Wilson, and W.-G. Zhu, 2005: Review of the link between the Hongge layered intrusion and Emeishan flood basalts, southwest China. *Int. Geol. Rev.*, **47**, 971-985, doi: 10.2747/0020-6814.47.9.971. [Link]

Zhong, H., I. H. Campbell, W.-G. Zhu, C. M. Allen, R.-Z. Hu, L.-W. Xie, and D.-F. He, 2011: Timing and source constraints on the relationship between mafic and felsic intrusions in the Emeishan large igneous province. *Geochim. Cosmochim. Acta*, **75**, 1374-1395, doi: 10.1016/j.gca.2010.12.016. [Link]

Zhou, M.-F., P. T. Robinson, C. M. Lesher, R. R. Keays, C.-J. Zhang, and J. Malpas, 2005: Geochemistry, petrogenesis and metallogenesis of the Panzhihua gabbroic layered intrusion and associated Fe-Ti-V oxide deposits, Sichuan Province, SW China. *J. Petrol.*, **46**, 2253-2280, doi: 10.1093/petrology/egi054. [Link]

Zhou, M.-F., N. T. Arndt, J. Malpas, C. Y. Wang, and A. K. Kennedy, 2008: Two magma series and associated ore deposit types in the Permian Emeishan large igneous province, SW China. *Lithos*, **103**, 352-368, doi: 10.1016/j.lithos.2007.10.006. [Link]

Zhou, M.-F., W. T. Chen, C. Y. Wang, S. A. Prevec, P. Liu, and G. H. Howarth, 2013: Two stages of immiscible liquid separation in the formation of Panzhihua-type Fe-Ti-V oxide deposits, SW China. *Geosci. Front.*, **4**, 481-502, doi: 10.1016/j.gsf.2013.04.006. [Link]